Journal of Porphyrins and Phthalocyanines
J. Porphyrins Phthalocyanines 2014; **18**: 259–266
DOI: 10.1142/S1088424614500114

Published at http://www.worldscinet.com/jpp/

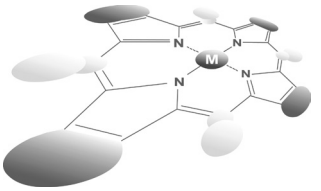

Self-organized one-dimensional columns of benzo[*b*]thiophene-fused tetraazaporphyrins

Hiroyuki Suzuki[a], Naoya Yamada[b], Ken-ichi Nakayama[b] and Mutsumi Kimura*[a◊]

[a] *Division of Chemistry and Materials, Faculty of Textile Science and Technology, Shinshu University, Ueda 386-8567, Japan*
[b] *Graduate School of Science and Engineering, Yamagata University, Yonezawa 992-8510, Japan*

Received 11 January 2014
Accepted 24 February 2014

ABSTRACT: Ring-expanded metallophthalocyanines fused with thiophene rings **1**–**4** have been synthesized by ring closing reaction from the *o*-chloroethynylbenzene substructures with Na_2S $9H_2O$. The self-organizing properties of these compounds have been studied by UV-vis spectroscopy in solution, π-A isotherms at air-water interface, X-ray diffraction (XRD) patterns of a solid, and atomic force microscopy (AFM). Whereas all compounds exhibit good solubility in organic solvents, thiophene-fused phthalocyanines form stable aggregates through strong intermolecular π–π interaction. Copper phthalocynaine Cu-**2** possessing phenyl spacers produced long nano-fibrous assemblies from solution.

KEYWORDS: metallophthalocyanines, ring closing reaction, one-dimensional column, self-organization, fibrous network.

INTRODUCTION

Large-area and flexible electronic devices fabricated by simple printing technologies using solution-based semiconducting materials have recently been attracting much intense attention due to their potential applications such as flexible displays, smart labels, and light-weight solar cells [1–6]. Various organic and inorganic semiconducting materials have been applied as functional inks for printed electronics. Among these semiconducting materials, well-defined thiophene-fused polycyclic aromatic derivatives with solubilizing groups exhibited excellent performance for organic-based electronic devices [7]. Takimiya *et al.* succeeded at systematic syntheses of solution-processable thiophene-fused aromatic derivatives. Solution-processed organic field-effect transistors (OFETs) fabricated by using solution-cast films of these materials have shown high field-effect mobility values above $1\,cm^2.V^{-1}.s^{-1}$ [8–11]. The molecular design of solution-processable organic semiconducting molecules requires long-range intermolecular orbital overlap in the solid state as well as high solubility in solution.

Phthalocyanines (Pcs) and their metal complexes (MPcs) have been used as molecular components in organic-based devices due to their intense absorbing Q-bands (600–700 nm), high molar extinction coefficients ($\varepsilon > 100{,}000\ M^{-1}.cm^{-1}$), and good thermal, chemical, and photochemical stabilities [12]. Extended flat hydrophobic Pc ligands, modified at either four or eight positions on each Pc with solubilizing side chains, can self-organize to form one-dimensional columns through intermolecular π–π stacking interactions [12]. The π–π overlap of MPcs within the columnar stacks provides a transport pathway for charge or energy parallel to the columnar axis. The long-range transportation of charge and energy in the columnar stacks can enhance the device performance of organic-based optical and electronic devices. The length of self-organized columns depends on the strength of intermolecular π–π stacking interactions among MPcs. In this context, many attempts have been made to control self-organization properties of MPcs by exploring molecular architecture of Pc ligand [13–18].

In this paper, we report syntheses of thiophene-fused MPc derivatives **1–4** through a ring closing reaction from the *o*-chloroethynylbenzene substructures, and

◊SPP full member in good standing

*Correspondence to: Mutsumi Kimura, email: mkimura@shinshu-u.ac.jp, tel/fax: +81 268-21-5499

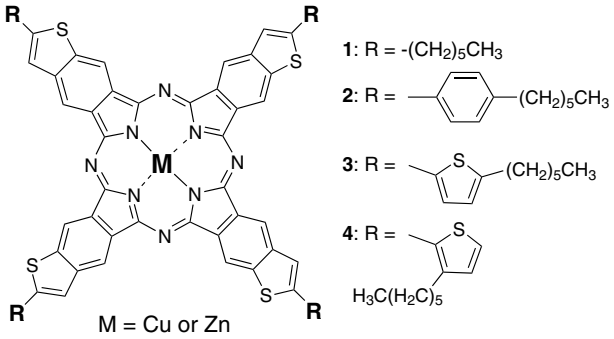

Fig. 1. Structure of thiophene-fused MPcs **1–4**. The structure is one of structural isomers

their self-organizing properties of ring-expanded MPcs in solution and a solid state (Fig. 1). Although several thiophene-fused tetraazaporphyrins have been synthesized, a benzothiophene-fused teteraazaporphyrin has not been reported [19–21]. The introduction of peripheral four alkyl chains with ring-expanded MPcs exhibits high solubility in organic solvents. Thiophene-fused Cu-**2** decorated with *n*-hexylphenyl substituents formed long fibrous aggregates through enhanced π–π interaction among ring-expanded MPcs. We also report preliminary results of the fabrication of OFETs using spin-coated thin films of Cu-**1** and Cu-**2** and the preparation of insoluble Pc-networked film by the electrochemical polymerization of Cu-**4**.

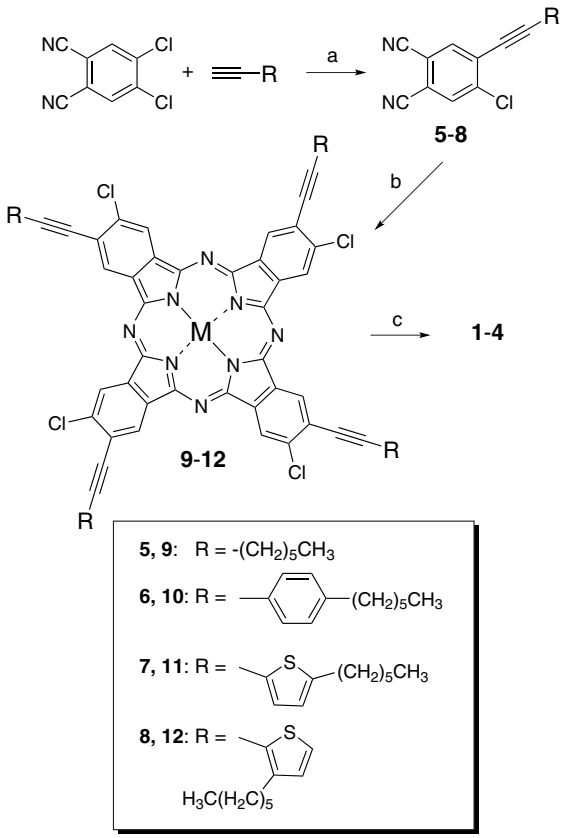

(a) $PdCl_2(PPh_3)_2$, CuI, triethylamine-THF, (b) $M(AcO)_2$, urea, *N,N'*-dimethylpropyleneurea, (c) Na_2S $9H_2O$, NMP. MPcs **1-4** and **9-12** contain structural isomers.

Scheme 1. M. Kimura *et al.*

RESULTS AND DISCUSSION

Scheme 1 illustrates the synthetic route of thiophene-fused MPcs **1–4**. Phthlocyanine precursors **5–8** were synthesized through palladium-catalyzed Sonogashira coupling of 4,5-dichlorophthalonitrile with alkynes. MPcs **9–12** fused with *o*-chloroethynylbenzene were prepared in the presence of metal salts, and the final ring closing reaction with sodium sulfide [22] obtained **1–4** in good yields. The MALDI-TOF-Ms spectra of all final compounds exhibit an expected parent molecular ion peak, and their purities were confirmed by HPLC analyses. All MPcs decorated with four flexible substituents at the α-positions of the fused thiophene rings revealed good solubility (>10 $g.L^{-1}$) in organic solvents such as THF, toluene and $CHCl_3$.

The shape and location of the Q-band of MPcs are known to be indicators for determining the aggregation behavior of MPcs. All CuPcs exhibit a broad absorption Q-band in the range of 550–850 nm in $CHCl_3$ (Fig. 2a and Table 1). The broadening of the Q-band is caused by exciton coupling between neighboring phthalocyanine rings in aggregates [23]. No changes on the absorption spectral shape in $CHCl_3$ were detected in the concentration range of 5 μM to 0.1 mM, indicating the formation of stable aggregates in solution. The absorption maxima of the Q-bands for thiophene-fused CuPcs **1–4** shift to longer wavelengths relative to the parent compounds. The red-shifting of Q-band is ascribed to the enlargement of the π-conjugated system by fusing thiophenes with the phthalocyanine ring. The Q-bands of Cu-**3** and Cu-**4** were red-shifted as compared with the spectra of Cu-**1** and Cu-**2** due to the attachment of electron-donating thiophene spacers with thiophene-fused phthalocyanine ring (Fig. S1). Figure 2b shows the absorption spectra of Cu-**1** and Cu-**2** in 1,3,5-trimethylbenzene. The spectrum of Cu-**1** in 1,3,5-trimethylbenzene displayed a peak at 733 nm, indicating the dissociation of aggregates into monomeric species caused by solvent changing. In contrast, the Q-bands of Cu-**2** remained unaltered in 1,3,5-trimethylbenzene. The aggregation properties in solution were enhanced by the presence of phenyl spacer in the solubilizing side chains. Whereas Cu-**1** exhibits a broad Q-band in $CHCl_3$, the peak at 734 nm is observed in the spectrum of Zn-**1** (Fig. 1c). The difference in the aggregation behavior reflected the attracting force between MPcs that had different central metals. The attracting force between CuPcs was stronger than that between ZnPcs.

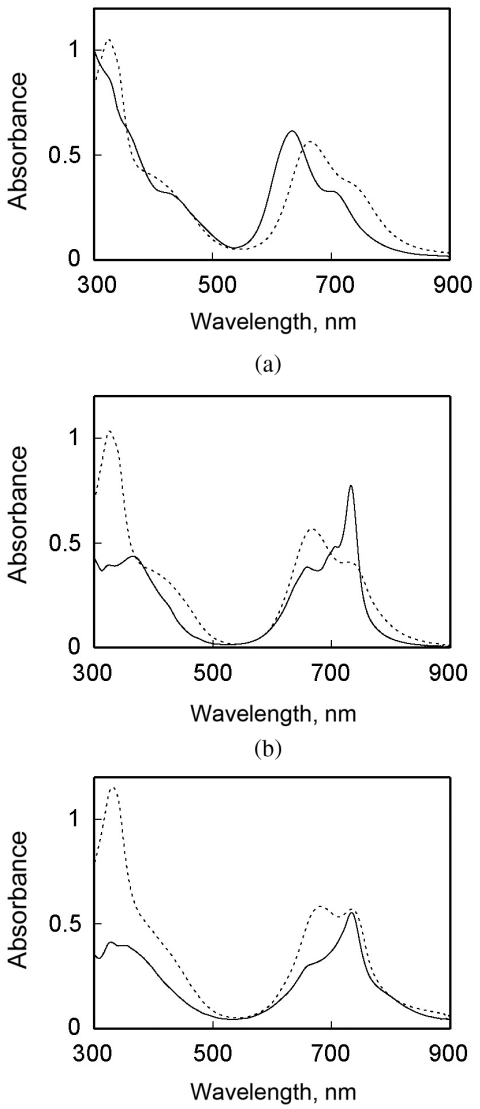

Fig. 2. Absorption spectra of (a) Cu-**10** (solid line) and Cu-**2** (dashed line) in $CHCl_3$, (b) Cu-**1** (solid line) and Cu-**2** (dashed line) in 1,3,5-trimethylbenzene, and (c) Zn-**1** (solid line) and Zn-**2** (dashed line) in $CHCl_3$. [MPcs] = 10 μM

Electrochemical studies of thiophene-fused MPcs were performed through cyclic voltammetry measurement in CH_2Cl_2 containing 0.1 M Bu_4NClO_4 as a supporting electrolyte (Table 1). Cu-**1** exhibits two reversible oxidation waves at +0.14 and +0.83 V *vs.* ferrocene/ferrocenium redox couple (*Fc/Fc*$^+$). Since Cu(II) does not undergo a redox process within the potential window in CH_2Cl_2, the observed oxidation processes can be ascribed to thiophene-fused phthalocyanine-centered ring oxidations [24]. The highest occupied molecular orbital (HOMO) energy levels of Cu-**1** and Cu-**2** were estimated to be -4.94 and -4.92 eV from the first oxidation potentials calibrated by the *Fc/Fc*$^+$ redox potential *vs.* vacuum (Table 1). The HOMO energy levels of Cu-**1** and Cu-**2** were slightly higher than that of copper phthalocyanines

Table 1. Photophysical and electrochemical data for MPcs **1–4**

Ligand	Metal	λ_{max}, nm[a]	$E_{1/2}$, V *vs. Fc/Fc*$^+$[b]
1	Cu	669, 726[sh]	0.14, 0.83
	Zn	670[sh], 734	0.14, 1.03
2	Cu	665, 740[sh]	0.12, 0.90
	Zn	682, 735	0.13, 1.14
3	Cu	672, 750[sh]	0.14, 1.02
4	Cu	677, 750[sh]	0.14, 1.02

[a] In $CHCl_3$. [b] Determined by differential pulse voltammetry in CH_2Cl_2 containing 0.1 M Bu_4NClO_4 at 295 K, scan rate = 50 mV/s [sh] Shoulder peak.

(HOMO = -5.2 eV). The enlargement of π-system resulted in the destabilization of the HOMO.

Phthalocyanines substituted with linear or branched alkyl, alkoxymethyl, or alkoxy chains form a major class of discotic liquid-crystalline materials that self-organize in columnar stacks [25–29]. The type of side chain, its length, the symmetry of Pc molecule influence the self-organized structure. The self-organizing properties of Cu-**1** and Cu-**2** were investigated by differential scanning calorimetry (DSC), temperature-controlled polarized optical microscopy (POM), and X-ray diffraction (XRD). No typical textures in POM and no transitions in DSC were observed in Cu-**1** and Cu-**2** on heating and cooling from -50 to 250 °C. The number and length of alkyl chains in Cu-**1** and Cu-**2** are not sufficient to exhibit liquid crystal phases. The XRD patterns of Cu-**1** and Cu-**2** at room temperature show one reflection peak corresponding to the *d* spacing of 2.23 and 2.53 nm, which is attributed to the average distance between stacked columns in the solid (Fig. S2). Cu-**2** with phenyl spacer has a longer average distance than Cu-**1**. Since the XRD patterns in the small angle region showed only one peak, two- or three-dimensional lattices could not be assigned from the XRD patterns. The reflection peak at 0.33 nm characteristic of the π–π stacking is observed, thus indicating a long-range ordering along the columnar axis. The broad and diffuse halo around 0.43 nm can be ascribed to the liquid-like disorder in alkyl chains.

The organized structures of Cu-**1** and Cu-**2** were analyzed by a surface pressure *vs.* area (π-A) isotherm on pure water as the substrate (Fig. 3) [30]. A continuous rise in the pressure as area decreased was observed up to 40 $mN.m^{-1}$, whereupon the monomolecular film collapsed. The limiting surface areas per molecules of Cu-**1** and Cu-**2** were 0.52 and 0.84 nm^2/molecule determined by extrapolating the slope of the π-A isotherms in the liquid-condensed region to zero pressure. The limiting surface area of Cu-**2** mostly agreed with the area occupied in an edge-on arrangement of molecules on the water surface. This indicates that Cu-**2** forms stacks with phthalocyanine plane perpendicular to the air-water interface. In contrast,

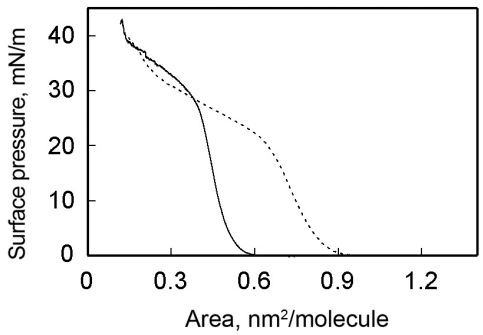

Fig. 3. Surface pressure *vs.* area per molecule isotherms for Cu-**1** (solid line) and Cu-**2** (dashed line) on triply distilled water at 25 °C

the limiting area of Cu-**1** is smaller than the estimated edge area (0.74 nm^2), suggesting the formation of slipped stacks on the interface [31].

The organized morphologies of Cu-**1** and Cu-**2** were visualized by atomic force scanning microscopy (AFM) (Fig. 4). A droplet of 5×10^{-5} M solutions of Cu-**1** or Cu-**2** in $CHCl_3$ was placed on a mica substrate, and the solution was evaporated in vacuum. Although the AFM height image of Cu-**1** shows no featured dots, Cu-**2** assembled into network structures of fibers with a 2.4 nm height. The fibers consist of bundles of finer strands, and some isolated single strands can be seen. The length of fibers is in an order of a few micrometers. The observed height of fibers is in fair agreement with the average intercolumnar distance as obtained from the XRD analysis and the diameter of molecular model of Cu-**2**. From these results, we may conclude that Cu-**2** self-assembles in $CHCl_3$ solution to produce long one-dimensional stacks. The phenyl spacers in Cu-**2** enhance the attracting force among molecules, and the enhanced attracting force induces the formation of nanoscopic fibers in solution. On the other hand, Cu-**1** assembles short stacks in solution relative to Cu-**2**. The short stacks result in the slipped stacks in air-water interface and the dotted structures on mica.

Solution-processed OFETs using Cu-**1** and Cu-**2** were fabricated using the top-contact device configuration. Thin films were deposited onto a Si/SiO_2 substrate with hydrophobic surface treatment using an insulating polymer by spin coating using 20 mg/mL solutions of Cu-**1** or Cu-**2** in $CHCl_3$ containing 1.0 wt% 1,3,5-trichlorobenzene at 1000 rpm for 40 sec. In AFM images, the obtained thin films appeared to be smooth and have a homogeneous surface with a surface roughness RMS of less than 0.3 nm in the region of 3 × 3 mm. Gold source and drain electrodes with 70 nm thickness were vapor-deposited on top of the thin films. The channel length and the width of the source and drain electrodes were 50 μm and 5.5 mm, respectively. FET characteristics were measured in a nitrogen glove box system. Both devices of Cu-**1** and Cu-**2** showed typical p-channel FET responses (Fig. 5). The field-effect mobilities measured in the saturation regime were 1.06×10^{-5} $cm^2.V^{-1}.s^{-1}$ for Cu-**1** and 2.37×10^{-5} $cm^2.V^{-1}.s^{-1}$ for Cu-**2** with I_{on}/I_{off} of 10^2–10^3. The device performance is lower than the reported values for phthalocyanine-based OFETs [19, 32–38]. The XRD patterns of spin-coated films on the Si/SiO_2 substrate revealed broad reflection peaks, indicating their low crystallinity. The low crystallinity of thin films results in low performance of OFETs.

Terminal α-positions of Cu-**4** are made available for electrochemical polymerization to produce cross-linked films. Electrochemical polymerization provides a convenient way for redox-active monomers to deposit a polymer film directly onto the surface of electrodes [39–41]. The electrochemical polymerization of Cu-**4** was performed in a three-electrode cell using platinum as a counter electrode, Ag/AgCl as a reference electrode, and ITO-coated glass substrate as a working electrode. Cu-**4** was electrodeposited as film using 0.1 mM concentration of CH_2Cl_2 containing 0.1 M Bu_4NPF_4 as a supporting electrolyte and scanning between -0.5 and 1.4 V at a scan rate of 50 mV/s. The polymer film of Cu-**4** on an ITO electrode was prepared by five cycles of potential scans. Two reversible oxidation waves at 0.53 and 1.04 V *vs.* Ag/AgCl were observed (Fig. 6a). The

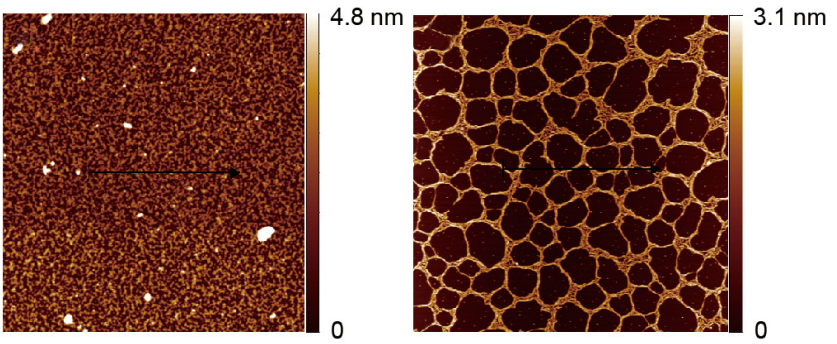

Fig. 4. AFM images (area: 5 × 5 μm) of (a) Cu-**1** and (b) Cu-**2** on mica substrates

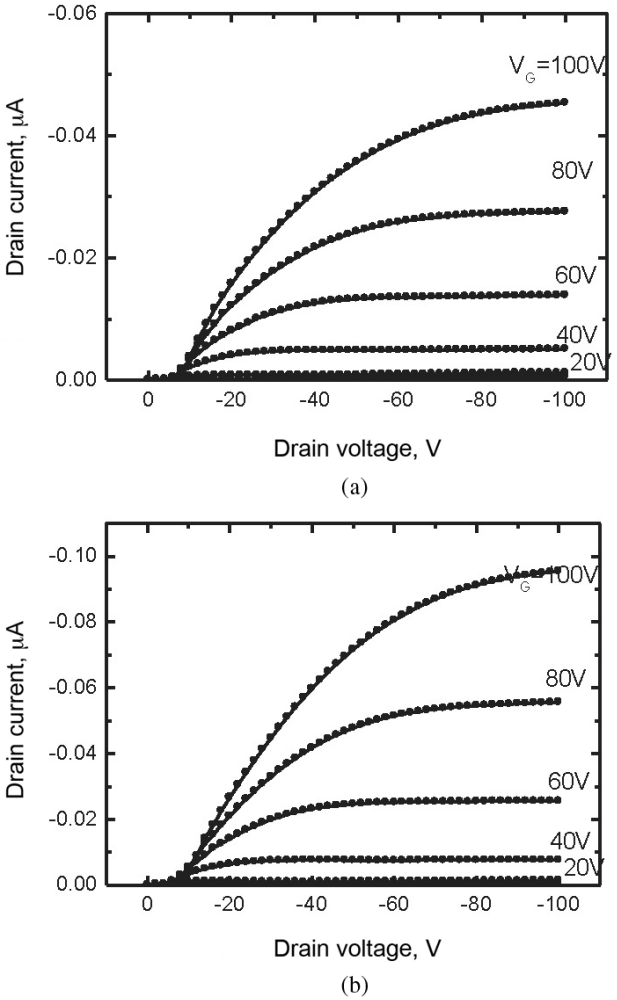

Fig. 5. Drain-source current *vs*. drain-source voltage characteristics for (a) Cu-**1** and (b) Cu-**2**

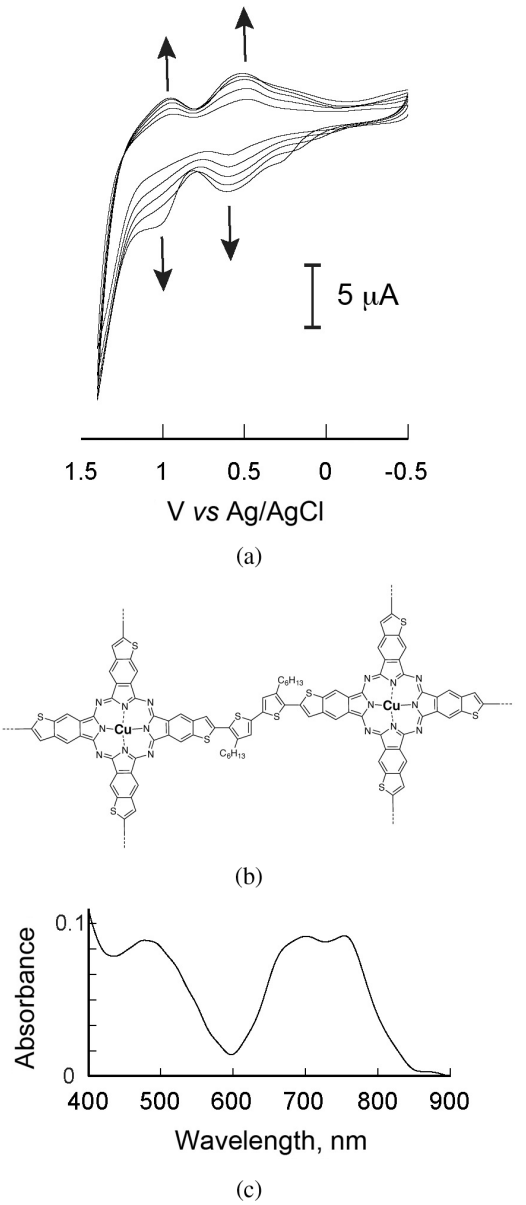

Fig. 6. (a) Repeated CV cycles of Cu-**4** in CH_2Cl_2 containing 0.1 M Bu_4NPF_4 (scan rate: 100 $mV.s^{-1}$). (b) Network structure of electropolymerized Cu-**4**. (c) Absorption spectrum of electropolymeized Cu-**4** deposited onto an ITO electrode

peak currents increased upon the repeated scans and a yellow-green film was deposited onto the surface of an ITO electrode. The resulting film on ITO is designated as polymerized Cu-**4**. Since four thiophene terminals in Cu-**4** could undergo the oxidative coupling reaction, the resulting polymers possess a three-dimensional network, where the thiophene-fused CuPcs are connected with bithiophene segments in the network polymer. The polymerized films were rinsed with CH_2Cl_2 to remove any residual soluble species (Fig. 6b). The rinsed films exhibited two oxidation waves at the same positions as observed in the electrochemical polymerization of Cu-**4**, and less than 5% loss of electroactivity after 50 repeated scans between 0 and 1.4 V in monomer-free electrolyte solution. The absorption spectrum of polymerized Cu-**4** is almost the same as that of Cu-**4** in solution, suggesting the stacking of CuPcs within the three-dimensional network (Fig. 6c) [42–44].

In summary, we have synthesized thiophene-fused phthalocyanines **1–4** through the ring closing reaction from the *o*-chloroethynylbenzene substructures. The self-organizing properties of thiophene-fused phthalocyanines were investigated in solution, at air-water interface, and in the solid state. The attachment of *n*-hexylphenyl units at α-positions of the fused thiophene rings creates the network structure of nanoscopic fibrous assemblies with excellent long-range stacking through the intermarocycle interaction with the additional interaction between peripheral phenyl spacers. Cu-**1** and Cu-**2** acted as a soluble p-channel organic semiconductor, but the field-effect mobility was not high due to the low crystallinity in the solid state. Cu-**4** possessing thiophene spacers was polymerized into the electrochemically active films onto an electrode by the connection of four

thiophene terminals through the oxidative coupling reaction. Further structural modifications of thiophene-fuse phthalocyanines to control molecular ordering in the solid phase are now underway in our group.

EXPERIMENTAL

General procedures

NMR spectra were recorded on a Bruker AVANCE 400 FT NMR spectrometer at 399.65 MHz and 100.62 MHz for ^{1}H and ^{13}C in $CDCl_3$ solution. Chemical shifts are reported relative to internal TMS. IR spectra were obtained on a SHIMAZU IR Prestige-21 with DuraSample IR II. UV-vis spectra were measured on a JASCO V-650. MALDI-TOF mass spectra were obtained on a Bruker autoflex spectrometer with dithranol as matrix.

All chemicals were purchased from commercial suppliers and used without purification. Column chromatography was performed with activated alumina (Wako, 200 mesh) or silica gel (Wakogel C-200). Recycling preparative gel permeation chromatography was carried out by a JAI recycling preparative HPLC using $CHCl_3$ as an eluent. Analytical thin layer chromatography was performed with commercial Merck plates coated with silica gel 60 F_{254} or aluminum oxide 60 F_{254}.

The transition temperatures were measured by differential scanning calorimetry with a SII DSC 6200 operated at a scanning rate of 10 °C.min^{-1} on heating and cooling. The apparatus was calibrated with indium as standard. The XRD patterns were obtained with a Rigaku XRD-DSC with Cu Kα radiation. Spacings were obtained from Bragg's law. Atomic force microscopy images were acquired in non-contact mode by a JEOL JSPM-5400 system.

Syntheses

Phthalonitriles

5. To a solution of 4,5-dichlorophthalonitrile (0.60 g, 3.05 mmol) and 1-octyne (0.50 g, 4.56 mmol) in triethylamine (4.0 mL) and THF (2.0 mL) was added $PdCl_2(PPh_3)_2$ (64 mg, 0.91 mmol) and Cu(I) (17 mg, 0.90 mmol). The reaction mixture was heated at 80 °C for 12 h under N_2 atmosphere. After cooling to room temperature, the reaction mixture was poured into water and extracted with CH_2Cl_2. The organic layer was dried over $MgSO_4$ and the solvent was evaporated. The residues was purified by column chromatography on silica gel by eluting with CH_2Cl_2 and *n*-hexane (1:1 v/v) and recycling preparative HPLC to give **5** (0.39 g, 47%). ^{1}H NMR ($CDCl_3$, 400.13 MHz): δ, ppm 7.82 (1H, s, ArH), 7.80 (1H, s, ArH), 2.53 (2H, t, J = 7.2 Hz, –CH_2–), 1.62–1.69 (2H, m, –CH_2–), 1.46–1.52 (2H, m, –CH_2–), 1.31–1.35 (4H, m, –CH_2–), 0.90 (3H, t, J = 7.2 Hz, –CH_3). ^{13}C NMR ($CDCl_3$, 100.61 MHz): δ, ppm 141.6, 137.7, 134.3, 130.4, 114.8, 114.7, 114.6, 114.4, 105.6, 75.9, 31.6, 28.9, 28.4, 22.9, 20.2, 14.4. IR (ATR): ν, cm^{-1} 2230 (–CN).

6. Compound **6** was synthesized from 4,5-dichlorophthalonitrile and 1-ethynyl-4-hexylbenzene by the same procedure of **1**. Yield 52%. ^{1}H NMR ($CDCl_3$, 400.13 MHz): δ, ppm 7.91 (1H, s, ArH), 7.83 (1H, s, ArH), 7.49 (2H, d, J = 8.4 Hz, ArH), 7.22 (2H, d, J = 8.4 Hz, ArH), 2.65 (2H, t, J = 7.6 Hz, –CH_2–), 1.58–1.66 (2H, m, –CH_2–), 1.28–1.35 (6H, m, –CH_2–), 0.89 (3H, t, J = 6.8 Hz, –CH_3). ^{13}C NMR ($CDCl_3$, 100.61 MHz): δ, ppm 146.4, 141.3, 137.4, 134.4, 132.5, 130.0, 129.3, 118.5, 115.0, 114.7, 114.6, 114.5, 103.1, 83.5, 36.5, 32.1, 31.5, 29.3, 23.0, 14.5. IR (ATR): ν, cm^{-1} 2230 (–CN).

7. Compound **7** was synthesized from 4,5-dichlorophthalonitrile and 2-ethynyl-5-hexylthiophene by the same procedure of **1**. Yield 42%. ^{1}H NMR ($CDCl_3$, 400.13 MHz): δ, ppm 7.88 (1H, s, ArH), 7.83 (1H, s, ArH), 7.27 (1H, d, J = 3.6 Hz, ArH), 6.76 (1H, d, J = 3.6 Hz, ArH), 2.84 (2H, t, J = 7.6 Hz, –CH_2–), 1.65–1.73 (2H, m, –CH_2–), 1.29–1.40 (6H, m, –CH_2–), 0.89 (3H, t, J = 6.8 Hz, –CH_3). ^{13}C NMR ($CDCl_3$, 100.61 MHz): δ, ppm 152.7, 140.6, 136.8, 135.4, 134.3, 129.8, 125.5, 118.3, 114.7, 114.6, 114.5, 96.9, 87.4, 31.9, 31.3, 30.8, 29.1, 22.9, 14.5. IR (ATR): ν, cm^{-1} 2232 (–CN).

8. Compound **8** was synthesized from 4,5-dichlorophthalonitrile and 2-ethynyl-3-hexylthiophene by the same procedure of **1**. Yield 25%. ^{1}H NMR ($CDCl_3$, 400.13 MHz): δ, ppm 7.89 (1H, s, ArH), 7.85 (1H, s, ArH), 7.37 (1H, d, J = 5.2 Hz, ArH), 6.96 (1H, d, J = 5.2 Hz, ArH), 2.81 (2H, t, J = 7.6 Hz, –CH_2–), 1.63–1.70 (2H, m, –CH_2–), 1.28–1.37 (6H, m, –CH_2–), 0.88 (3H, t, J = 6.8 Hz, –CH_3). ^{13}C NMR ($CDCl_3$, 100.61 MHz): δ, ppm 152.1, 140.4, 136.7, 134.4, 130.0, 129.8, 129.2, 116.4, 114.7, 114.6, 96.4, 90.3, 32.0, 30.7, 30.3, 29.4, 23.0, 14.5. IR (ATR): ν, cm^{-1} 2232 (–CN).

Phthalocyanines

Cu-9. A mixture of **5** (150 mg, 0.55 mmol), urea (67 mg, 1.1 mmol), and $Cu(OAc)_2$ H_2O (28 mg, 0.14 mmol) in *N*,*N*′-dimethylpropyleneurea (3.0 mL) was heated at 160 °C for 12 h under N_2 atmosphere. After cooling to 60 °C, methanol was added to the reaction mixture and stirred for 15 min. The resulting suspension was filtered off and washed with methanol. The solid residue was purified by column chromatography on activated alumina by eluting with $CHCl_3$ and recycling preparative HPLC to give Cu-**9** (53 mg, 33%). UV-vis (10 μM in $CHCl_3$): λ, nm 628 and 695. MALDI-TOF MS (dithranol): *m/z* 1146.5 ([M + H], 100%), calcd. for $C_{64}H_{60}Cl_4N_8Cu$: *m/z* 1146.6.

Zn-9. Zn-**9** was synthesized from **5** and $Zn(OAc)_2$ by the same procedure of Cu-**9**. Yield 55%. UV-vis (10 μM in $CHCl_3$): λ, nm 696. ^{1}H NMR ($CDCl_3$, 400.13 MHz): δ, ppm 8.5–9.0 (4H, br, ArH), 6.4–6.7 (4H, br, ArH), 2.7–2.9 (8H, m, –CH_2–), 1.7–2.0 (16H, m, –CH_2–), 1.0–1.2

(16H, m, $–CH_2–$), 0.8 (12H, br, $–CH_3$). MALDI-TOF MS (dithranol): *m/z* 1148.4 ([M + H], 100%), calcd. for $C_{64}H_{60}Cl_4N_8Zn$: *m/z* 1148.4.

Cu-10. Cu-**10** was synthesized from **6** and $Cu(OAc)_2 H_2O$ by the same procedure of CuCu-**9**. Yield 49%. UV-vis (10 μM in $CHCl_3$): λ, nm 634 and 710^{sh}. MALDI-TOF MS (dithranol): *m/z* 1449.2 ([M + H], 100%), calcd. for $C_{88}H_{76}Cl_4N_8Cu$: *m/z* 1450.9.

Zn-10. Yield 51%. UV-vis (10 μM in $CHCl_3$): λ, nm 655 and 705. ^{1}H NMR ($CDCl_3$, 400.13 MHz): δ, ppm 6.4–9.0 (24H, br, ArH), 3.5–3.9 (8H, m, $–CH_2–$), 2.3–2.6 (8H, m, $–CH_2–$), 1.6–1.9 (8H, m, $–CH_2–$), 1.2–1.4 (16H, m, $–CH_2–$), 0.8 (12H, br, $–CH_3$). MALDI-TOF MS (dithranol): *m/z* 1452.2 ([M + H], 100%), calcd. for $C_{88}H_{76}Cl_4N_8Zn$: *m/z* 1452.8.

Cu-11. Cu-**11** was synthesized from **7** and $Cu(OAc)_2 H_2O$ by the same procedure of CuCu-**9**. Yield 49%. UV-vis (10 μM in $CHCl_3$): λ, nm 644 and 712^{sh}. MALDI-TOF MS (dithranol): *m/z* 1472.7 ([M + H], 100%), calcd. for $C_{80}H_{68}Cl_4N_8S_4Cu$: *m/z* 1471.2.

Cu-12. Cu-**12** was synthesized from **8** and $Cu(OAc)_2 H_2O$ by the same procedure of CuCu-**9**. Yield 66%. UV-vis (10 μM in $CHCl_3$): λ, nm 648 and 711. MALDI-TOF MS (dithranol): *m/z* 1473.7 ([M + H], 100%), calcd. for $C_{80}H_{68}Cl_4N_8S_4Cu$: *m/z* 1471.2.

Thiophene-fused phthalocyanines

Cu-1. A mixture of Cu-**9** (27 mg, 0.23 μmol), $NaS 9H_2O$ (45 mg, 18.8 μmol) in *N*-methylpyrrolidone (5.0 mL) was stirred at 190 °C with stirring for 12 h under N_2 atomosphere. After cooling to room temperature, the reaction mixture was poured into 50 mL saturated NH_4Cl aqueous solution and stirred for 30 min. The resulting suspension was filtered off and washed with methanol. The solid residue was purified by column chromatography on activated alumina by eluting with $CHCl_3$ and recycling preparative HPLC to give Cu-**1** (11 mg, 41%). UV-vis (10 μM in $CHCl_3$): λ, nm 669 and 726. MALDI-TOF MS (dithranol): *m/z* 1135.1 ([M + H], 100%), calcd. for $C_{64}H_{64}N_8S_4Cu$: *m/z* 1135.4. Elemental analysis calcd. (%) for $C_{64}H_{64}N_8S_4Cu$: C 67.60, H 5.67, N 9.85; found C 67.7, H 5.7, N 9.7. Purity (HPLC) > 99%.

Zn-**1**, Cu-**2**, Zn-**2**, Cu-**3**, and Cu-**4** were synthesized by the same procedure of Cu-**1**.

Zn-1. Yield 24%. UV-vis (10 μM in $CHCl_3$): λ, nm 670^{sh} and 734. ^{1}H NMR ($CDCl_3$, 400.13 MHz): δ, ppm 6.6–8.5 (12H, br, ArH), 3.6–3.8 (16H, m, $–CH_2–$), 2.0 (8H, br, $–CH_2–$), 1.3 (16H, br, $–CH_2–$), 0.7 (12H, br, $–CH_3$). MALDI-TOF MS (dithranol): *m/z* 1137.3 ([M + H], 100%), calcd. for $C_{64}H_{64}N_8S_4Zn$: *m/z* 1136.3. Elemental analysis calcd. (%) for $C_{64}H_{64}N_8S_4Zn$: C 67.50, H 5.66, N 9.84; found C 67.6, H 5.6, N 9.7. Purity (HPLC) > 99%.

Cu-2. Yield 36%. UV-vis (10 μM in $CHCl_3$): λ, nm 665 and 740^{sh}. MALDI-TOF MS (dithranol): *m/z* 1441.4 ([M + H], 100%), calcd. for $C_{88}H_{80}N_8S_4Cu$: *m/z* 1441.4. Elemental analysis calcd. (%) for $C_{88}H_{80}N_8S_4Cu$: C 73.33, H 5.59, N 7.77; found C 73.4, H 5.6, N 7.8. Purity (HPLC) > 99%.

Zn-2. Yield 25%. UV-vis (10 μM in $CHCl_3$): λ, nm 682 and 735. ^{1}H NMR ($CDCl_3$, 400.13 MHz): δ, ppm 6.6–8.5 (28H, br, ArH), 3.6–3.8 (8H, m, $–CH_2–$), 2.4–2.6 (8H, m, $–CH_2–$), 1.9 (8H, br, $–CH_2–$), 1.3 (16H, br, $–CH_2–$), 0.9 (12H, br, $–CH_3$). MALDI-TOF MS (dithranol): *m/z* 1443.4 ([M + H], 100%), calcd. for $C_{88}H_{80}N_8S_4Zn$: *m/z* 1443.3. Elemental analysis calcd. (%) for $C_{88}H_{80}N_8S_4Zn$: C 73.23, H 5.59, N 7.76; found C 73.3, H 5.6, N 7.7. Purity (HPLC) > 99%.

3. Yield 50%. UV-vis (10 μM in $CHCl_3$): λ, nm 670^{sh} and 734. MALDI-TOF MS (dithranol): *m/z* 1463.3 ([M + H], 100%), calcd. for $C_{80}H_{72}N_8S_8Cu$: *m/z* 1463.3. Elemental analysis calcd. (%) for $C_{80}H_{72}N_8S_8Cu$: C 65.57, H 4.95, N 7.65; found C 65.5, H 5.0, N 7.6. Purity (HPLC) > 99%.

4. Yield 43%. UV-vis (10 μM in $CHCl_3$): λ, nm 682 and 735. MALDI-TOF MS (dithranol): *m/z* 1464.7 ([M + H], 100%), calcd. for $C_{80}H_{72}N_8S_8Cu$: *m/z* 1463.3. Elemental analysis calcd. (%) for $C_{80}H_{72}N_8S_8Cu$: C 65.57, H 4.95, N 7.65; found C 65.6, H 4.9, N 7.7. Purity (HPLC) > 99%.

Acknowledgements

This work has been partially supported by Grants-in-Aid for Scientific Research (B) (No. 22350086) from Japan Society for the Promotion of Science (JSPS).

Supporting information

Figures S1 and S2 are given in the supplementary material. This material is available free of charge *via* the Internet at http://www.worldscinet.com/jpp/jpp.shtml.

REFERENCES

1. Arias AC, MacKenzie JD, McCulloch I, Rivnay J and Salleo A. *Chem. Rev.* 2010; **110**: 3.
2. Habas S, Platt HAS, van Hest FAM and Ginley DS. *Chem. Rev.* 2010; **110**: 6571.
3. Wen Y, Liu Y, Guo Y, Yu G and Hu W. *Chem. Rev.* 2011; **111**: 3358.
4. Mas-Torrent M and Rovira C. *Chem. Rev.* 2011; **111**: 4833.
5. Minemawari H, Yamada T, Matsui H, Tsutsumi J, Haas S, Chiba R, Kumai R and Hasegawa T. *Nature* 2011; **475**: 364.
6. Babu SS, Prasanthkumar S and Ajayaghosh A. *Angew. Chem. Int. Ed.* 2011; **51**: 1766.
7. Takimiya K, Shinamura S, Osaka I and Miyazaki E. *Adv. Mater.* 2011; **23**: 4347 and related references therein.
8. Takimiya K, Kunugi Y, Konda Y, Niihara N and Otsubo T. *J. Am. Chem. Soc.* 2004; **126**: 5084.

9. Ebata H, Izawa T, Miyazaki E, Takimiaya K, Ikeda M, Kuwabara H and Yui T. *J. Am. Chem. Soc.*, 2007; **129**: 15732.
10. Izawa T, Miyazaki E and Takimiya K. *Adv. Mater.* 2008; **20**: 3388.
11. Shinamura S, Osaka I, Miyazaki E, Nakao A, Yamagishi M, Takeya J and Takimiya K. *J. Am. Chem. Soc.* 2011; **133**: 5024.
12. Kaafarani BR. *Chem. Mater.* 2011; **23**: 378.
13. van Nostrum CF, Picken SJ, Schouten AJ and Nolte RJM. *J. Am. Chem. Soc.* 1995; **117**: 9957.
14. Smolenyak P, Peterson R, Nebesny K, Törker M, O'Brien DF and Armstrong NR. *J. Am. Chem. Soc.* 1999; **121**: 8628.
15. Kimura M, Muto T, Takimoto H, Wada K, Ohta K, Hanabusa K, Shirai H and Kobayashi N. *Langmuir* 2000; **16**: 2078.
16. Kimura M, Wada K, Ohta K, Hanabusa K and Shirai H. *J. Am. Chem. Soc.* 2001; **123**: 2438.
17. de la Escosura A, Martínez-Díaz MV, Thordarson P, Rowan AE, Nolte RJM and Torres T. *J. Am. Chem. Soc.* 2003; **125**: 12300.
18. Cook MJ and Jafari-Fini A. *J. Mater. Chem.* 1997; **7**: 5.
19. Miyazaki E, Kaku A, Mori H, Iwatani M and Takimiya K. *J. Mater. Chem.* 2009; **19**: 5913.
20. Taraimovich ES, Stuzhin PA and Koifman OI. *Russ. J. Gen. Chem.* 2013; **83**: 392.
21. Dubinina TV, Dyumaeva DV, Trashin SA, Sedova MV, Dudnik AS, Borisova NE, Tomilova LG and Zefirov N. *Dyes Pigm.* 2013; **96**: 699.
22. Kashiki T, Shinamura S, Kohara M, Miyazaki E, Takimiya K, Ikeda M and Kuwabara H. *Org. Lett.* 2009; **11**: 2473.
23. Stillman MJ and Nyokong T. *Phthalocyanines Properties and Applications*, Vol. 1, Leznoff CC and Lever ABP. (Eds.) VCH: New York, 1989; pp 135.
24. Lever ABP, Milaeva ER and Speier G. *Phthalocyanines Properties and Applications*, Vol. 3, Leznoff CC and Lever ABP. (Eds.) VCH: New York, 1993; pp 3.
25. Piechocki C, Simon J, Skoulios A, Guillon D and Weber P. *J. Am. Chem. Soc.* 1982; **104**: 5245.
26. Clarkson GJ, Cook A, McKeown NB, Treacher K and Ali-Adib Z. *Macromolecules* 1996; **29**: 913.
27. Ohta K, Yamaguchi N and Yamamoto I. *J. Mater. Chem.* 1998; **8**: 2637.
28. Kimura M, Kuroda T, Ohta K, Hanabusa K, Shirai H and Kobayashi N. *Langmuir* 2003; **19**: 4825.
29. De Cupere V, Tant J, Viville P, Lazzaroni R, Osikowicz W, Salaneck WR and Geerts YH. *Langmuir* 2006; **22**: 7798.
30. Cook MJ and Chambrier I. *The Porphyrin Handbook*, Vol. 17, Kadish KM, Smith KM and Guilard R. (Eds.) Academic Press: San Diego, CA, 2000; pp 37.
31. Kobayashi N, Lam H, Nevin WA, Janda P, Leznoff CC, Koyama T, Monden A and Shirai H. *J. Am. Chem. Soc.* 1994; **116**: 879.
32. Bao Z, Lovinger AJ and Dodabalapur A. *Appl. Phys. Lett.* 1996; **69**: 3066.
33. Bao Z, Lovinger AJ and Brown J. *J. Am. Chem. Soc.* 1998; **120**: 207.
34. Xiao K, Liu Y, Huang X, Xu Y, Yu G and Zhu D. *J. Phys. Chem. B* 2003; **107**: 9226.
35. Zhang J, Wang J, Wang H and Yan D. *Appl. Phys. Lett.* 2004; **84**: 142.
36. Su W, Jiang J, Xiao K, Chen Y, Zhao Q, Yu G and Liu Y. *Langmuir* 2005; **21**: 6527.
37. Tang ML, Oh JH, Reichardt AD and Bao Z. *J. Am. Chem. Soc.* 2009; **131**: 3733.
38. Kim Sh, Ko HC, Moon B and Lee H. *Langmuir* 2006; **22**: 9431.
39. Ponnapati R, Felipe MJ and Advincula R. *Macromolecules* 2011; **44**: 7530.
40. Kimura M, Sakai R, Sato S, Fukawa T, Ikehara T, Maeda R and Mihara T. *Adv. Funct. Mater.* 2012; **22**: 469.
41. Liu TA, Prabhakar C, Yu JY, Chen Ch, Huang HH and Yang JS. *Macromolecules* 2012; **45**: 4529.
42. Kimura M, Horai T, Hanabusa K and Shirai H. *Chem. Lett.* 1997; **26**: 653.
43. Obirai J, Rodrigues NP, Bedioui F and Nyokong T. *J. Porphyrins Phthalocyanines* 2003; **7**: 508.
44. Kimura M, Yasuta K, Adachi N, Tatewaki Y, Fukawa T and Shirai H. *Chem. Lett.* 2009; **38**: 82.